Electro-Opto-Mechanical Microwave-Frequency Oscillator in a Surface Acoustic Wave Silicon-Photonic Circuit

Maayan Priel
Faculty of Engineeing and Institute for Nano-Technology and Advanced Materials
Bar-Ilan University
Ramat-Gan, Israel
lmaayanl@gmail.com

Saawan Kumar Bag
Faculty of Engineeing and Institute for Nano-Technology and Advanced Materials
Bar-Ilan University
Ramat-Gan, Israel
saawanbagn7@gmail.com

Matan Slook
Faculty of Engineeing and Institute for Nano-Technology and Advanced Materials
Bar-Ilan University
Ramat-Gan, Israel
matanslook@gmail.com

Leroy Dokhanian
Faculty of Engineeing and Institute for Nano-Technology and Advanced Materials
Bar-Ilan University
Ramat-Gan, Israel
leroydok@gmail.com

Inbar Shafir
Faculty of Engineeing and Institute for Nano-Technology and Advanced Materials
Bar-Ilan University
Ramat-Gan, Israel
inbarsh@soreq.gov.il

Etai Grunwald
Faculty of Engineeing and Institute for Nano-Technology and Advanced Materials
Bar-Ilan University
Ramat-Gan, Israel
etaigrunwald@gmail.com

Moshe Katzman
Faculty of Engineeing and Institute for Nano-Technology and Advanced Materials
Bar-Ilan University
Ramat-Gan, Israel
moshekatzman111@gmail.com

Mirit Hen
Faculty of Engineeing and Institute for Nano-Technology and Advanced Materials
Bar-Ilan University
Ramat-Gan, Israel
mirithen071110@gmail.com

Avi Zadok
Faculty of Engineeing and Institute for Nano-Technology and Advanced Materials
Bar-Ilan University
Ramat-Gan, Israel
Avinaom.Zadok@biu.ac.il

2022 IEEE International Topical Meeting on Microwave Photonics (MWP) | 978-1-6654-2121-8/22/$31.00 ©2022 IEEE | DOI: 10.1109/MWP54208.2022.9997729

***Abstract*—An electro-opto-mechanical microwave frequency oscillator is demonstrated through a silicon photonic circuit. An electrical signal modulates an optical pump wave input. Modulation is converted to a surface acoustic wave on the silicon circuit through absorption in a metallic grating and thermoelastic expansion. The acoustic wave is delayed and converted back to optics through photoelastic modulation of a continuous optical input probe wave in a racetrack resonator waveguide. The output probe is detected, and the obtained voltage is amplified and fed back to modulate the input optical pump wave. With sufficient feedback gain, the electro-opto-mechanical loop is driven to oscillations at 2.21 GHz frequency. The oscillator can be useful for integrated microwave photonics signal processing.**

Keywords—silicon photonics, microwave photonics, surface acoustic waves, oscillators, integrated devices.

I. Introduction

Opto-electronic oscillators are sources of microwave-frequency tones that can reach very low noise levels [1-3]. In a typical arrangement, an electrical waveform modulates an optical carrier at the input of an optical waveguide [1-3]. The waveform is delayed in the optical medium and detected back into the electrical domain at the output end. The received voltage is amplified and fed back to modulate the optical input. Given sufficient electrical and/or optical gain, the closed loop may be driven into steady-state oscillations. Opto-electronic oscillators are often based on long fiber paths [1-3].

Much effort has been dedicated to device level realizations of opto-electronic oscillators. Examples include Brillouin active waveguides [4], whispering gallery mode lithium niobate resonators [5], and the integration of laser sources, delay waveguides, modulation, and detection in an indium-phosphide photonic circuit [6]. In other works, sharp spectral filters, modulators, and detectors were implemented in a silicon-photonic circuit [7,8].

Radio-frequency oscillators are also implemented based on electro-mechanics [9,10]. An input voltage is applied to an array of inter-digital electrodes on a piezoelectric material. A surface acoustic wave is launched and propagated along the substrate. The acoustic wave is reconverted to an electrical signal using a second set of electrodes in the far end [9,10]. The output signal is amplified and provides feedback to the input array. Closed loop electro-mechanical oscillators are suitable for device level integration. In quartz micro balance devices [7,8], the exact frequency of oscillations is used to precisely monitor the thickness of deposited layers [9,10]. The frequencies of operation are typically in the hundreds of MHz range. The electrical interfaces of the devices might not be suitable for certain environments.

Over the last four years, our group has developed surface acoustic wave (SAW) photonic devices within standard silicon on insulator circuits [11-14]. The devices serve as integrated radio-frequency filters. Incoming microwave-rate information is modulating an optical pump carrier wave. The information is converted to a SAW through thermoelastic actuation: the absorption of the modulated pump light in a metallic grating and subsequent thermal expansion [15,16]. The slow-moving acoustic waves accumulate long delays within compact devices. Information is recovered in the optical domain through photoelastic modulation of a continuous optical probe wave within a standard resonator waveguide, and it is detected at the probe output [11-14]. Both the thermoelastic actuation and the photoelastic modulation are frequency selective. SAW-photonic, microwave filters with a single passband that is only 7 MHz wide were realized

using this platform [14]. Similar to quartz micro-balance devices, the SAW-photonic circuits also served in the analysis of deposited thin layers [13].

In this work, we report an electro-opto-mechanical, microwave-frequency oscillator based on the SAW-photonic platform. The detected voltage of the output probe wave is electrically amplified and fed back to modulate the pump input. Sufficient gain drives the circuit into oscillations at 2.21 GHz frequency, much higher than conventional quartz micro-balance devices. The frequency of oscillations is pre-determined by the spatial period of the metallic grating element. Thresholds of oscillations are observed with respect to the input power of the optical probe wave and the alignment of its wavelength to the spectral slope of the resonator waveguide transfer function. The results successfully carry over the concept of electro-opto-mechanical oscillators, previously demonstrated through Brillouin scattering over fiber [17,18], to an integrated-photonic platform. The devices may serve in precision analysis of mass loading and thin layer deposition within photonic circuits, and in integrated microwave photonic signal processing.

II. Principle of Operation

A schematic illustration of the SAW-photonic microwave frequency oscillator is shown in Fig. 1. We analyze the propagation of signals along the electro-opto-mechanical loop subject to steady state oscillations at radio frequency Ω. A voltage of magnitude $V(\Omega)$ is applied to an electro-optic Mach-Zehnder intensity modulator of known V_π. Pump light from a first laser diode is intensity modulated by the voltage signal and amplified to an average optical power $\bar{P}_p$. The magnitude of the pump wave modulation [W] is given by $\delta P_p(\Omega) = \bar{P}_p J_1[\pi V(\Omega)/V_\pi]$, where J_1 is the first-order Bessel function of the first kind.

The modulated pump wave is absorbed in a grating of thin metallic stripes of length l and spatial period $\Lambda = 2\pi v_{ph}/\Omega$, where v_{ph} is the phase velocity of SAWs in the silicon-on-insulator layer stack. Periodic thermal expansion and contraction of the grating elements lead to the launch of SAWs away from the grating region. The thin metallic stripes thermalize within picoseconds [15,16]. The SAWs propagate across the straight sections of a racetrack resonator waveguide and induce perturbations to the effective index of guided light with a magnitude $\Delta n(\Omega) = C \cdot \delta P_p(\Omega)$ refractive index units (RIU). Here $C \sim 10^{-6}$ RIU×W^{-1} is a coefficient that depends on thermoelastic characteristics of the metallic grating, photoelastic properties of the silicon-on-insulator layers, and the transverse profile of the optical mode in the resonator waveguide [12].

Continuous probe light from a second laser diode is coupled to the racetrack resonator waveguide. Photoelastic index perturbations lead to phase modulation of the probe wave in both straight waveguide sections of the resonator [11-14]. The acoustic propagation delay τ between the two straight waveguides is chosen so that $\Omega\tau$ equals an integer multiple of 2π. The magnitude of phase modulation equals $\Delta\varphi(\Omega) = 2lk_0\Delta n(\Omega)$, where k_0 is the vacuum wavenumber of the probe wave [11-14]. The probe wavelength is carefully aligned to a maximal slope of the optical power transfer function of the racetrack resonator. With that choice, the photoelastic perturbations are converted to intensity modulation of the output probe wave, with magnitude $\delta P_s(\Omega) = 4Q\bar{P}_s(l/L)[\Delta n(\Omega)/n_g]$ [9]. Here $\bar{P}_s$ is the mean output power of the probe wave, Q is the quality factor of the racetrack resonator, L is its circumference, and n_g denotes the group refractive index of guided light.

The modulated optical probe wave at the device output is detected by a photo-receiver of responsivity R [V×W^{-1}]. The detected signal $\delta V(\Omega) = R \cdot \delta P_s(\Omega)$ is amplified by a radio frequency amplifier of small-signal voltage gain G, and the output voltage $G \cdot \delta V(\Omega)$ is fed back to modulate the input optical pump wave. Steady state oscillations are obtained when $G \cdot \delta V(\Omega) = V(\Omega)$. This condition is met when [18]:

$$V(\Omega) = 4GRQ\bar{P}_s[l/(n_g L)]C\bar{P}_p J_1[\pi V(\Omega)/V_\pi] \quad (1)$$

A threshold condition for small signals may be found by approximating $J_1(x) \approx x/2$. Signals are coupled out of the loop using optical or electrical taps (Fig. 1).

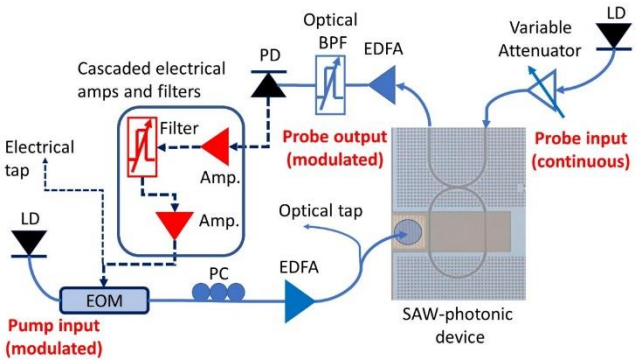

Fig. 1. Schematic illustration of an electro-opto-mechanical oscillator setup based on a surface acoustic wave-photonic device in silicon-on-insulator. EDFA: erbium-doped fiber amplifier; PC: polarization controller; EOM: electro-optic Mach-Zehnder intensity modulator; Amp.: Radio-frequency electrical amplifier; LD: laser diode; PD: photodetector; BPF: bandpass filter.

III. Experimental Results

Racetrack waveguides were fabricated in 8" silicon-on-insulator wafers by Tower Semiconductors foundry in northern Israel [12,13]. The thicknesses of the silicon device layer and the buried oxide layer were 220 nm and 2 µm, respectively. Patterns were defined using UV stepper photolithography and inductively coupled plasma reactive ion etching. The waveguides cross-section was of ridge geometry, with partial etching depth of 70 nm and width of 700 nm. The racetrack circumference L was 480 µm, and the group refractive index n_g of the guided optical mode was approximately 3.5 RIU.

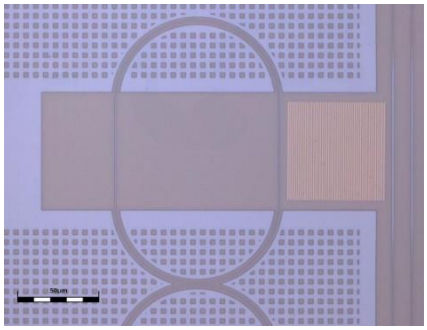

Fig. 2. Top-view optical microscope image of a surface acoustic wave-photonic device used in an electro-opto-mechanical oscillator. The scale bar corresponds to 50 µm.

Metallic gratings of 5 nm thick chromium adhesion layer and 20 nm thick gold layer were fabricated at Bar-Ilan University using electron beam lithography, sputtering, and lift-off processes [11-14]. The length l and period Λ of the gratings were 60 μm and 1.49 μm, respectively. A top-view microscope image of a SAW-photonic device is shown in Fig. 2. Light was coupled between standard single-mode fibers and the bus waveguides of devices under test using vertical grating couplers. Coupling losses were 10 dB per facet. Figure 3 shows an optical vector network analyzer measurement of the transfer function of optical power through a racetrack resonator device. The Q factor of the device was 150,000 and the extinction ratio of its transfer function was 7 dB. End-to-end transmission losses of optical power at off-resonance wavelengths were 29 dB.

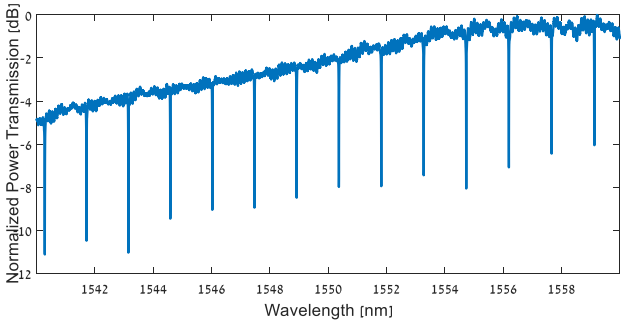

Fig. 3. Measured normalized transfer function of optical power through a racetrack resonator within a surface acoustic wave-photonic device as a function of wavelength.

Figure 4 presents the transfer function of radio-frequency electrical power between the modulation of the input pump wave and that of the detected output probe wave. The average pump power $\bar{P}_p$ was 600 mW, and V_π of the modulator was 3.5 V. The responsivity of the photodetector used was 27 V×W^{-1}. To obtain this transfer function, the electrical feedback between input and output was replaced by a radio-frequency electrical vector network analyzer. The pump wave modulator was driven by the output port of the network analyzer, and the detected probe output signal was monitored by the analyzer input port. A tunable optical bandpass filter at the detector input was used to suppress the amplified spontaneous emission of optical amplifiers.

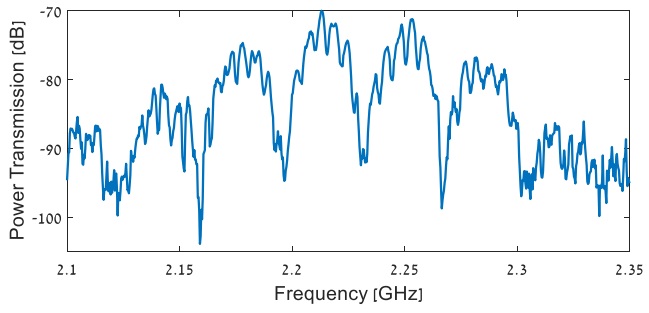

Fig. 4. Measured open-loop transfer function of radio-frequency electrical power between the modulation of the input pump wave and that of the detected output probe wave.

The transfer function of the device is maximal at 2.213 GHz frequency, for which $\Lambda = 2\pi v_{ph}/\Omega$ [11-14]. A spectral envelope of 100 MHz bandwidth corresponds to the frequency response of thermo-elastic actuation [14]. Periodic passbands with a free spectral range of 35 MHz are observed within the stimulation envelope. The free spectral range corresponds to an acoustic delay τ of 28 ns between the two straight sections of the racetrack resonator [11-14]. A narrower overlaying spectral periodicity of 6 MHz is observed within each primary passband (Fig. 2). This spectral modulation is possibly dye to the stimulation of bulk acoustic waves downward into the silicon substrate and their delayed reflection from its bottom surface. Losses of electrical radio-frequency power between the modulation of the pump input and that of the probe output at the frequency of maximum transmission were 70 dB.

Next, the electrical vector network analyzer was removed, and the loop was closed through a cascaded chain of four radio-frequency electrical amplifiers in series. The voltage gain G of the amplifiers chain was 60,000 (electrical power gain of 96 dB). Tunable bandpass filters with a central frequency of 2.21 GHz and 20 MHz bandwidth were placed at the outputs of the photodetector and of the first, third and fourth amplifiers in the series, to prevent saturation by accumulated broadband noise. Measurements were taken using an electrical splitter tap, located at the output of the final amplifier in the series.

Figure 5 shows radio-frequency power spectra of the loop output signal for several values of the probe power at the input of the resonator waveguide. For low probe power levels, broadband noise that follows the spectral shape of the cascaded radio-frequency filters is observed. As the probe power is gradually increased, periodic peaks emerge with a free spectral range of 1.2 MHz. The peaks represent longitudinal modes of the electro-opto-mechanical loop. The free spectral range corresponds to a loop group delay of 830 ns, which combines both optical and electrical paths and delays within radio-frequency amplifiers and bandpass filters.

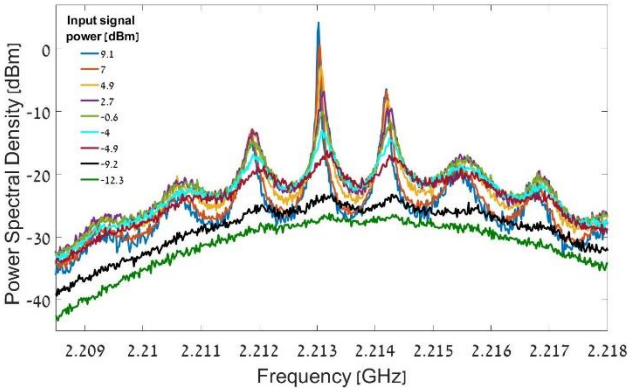

Fig. 5. Measured power spectral density of the loop output signal, for several optical power levels of the probe wave at the input of the photonic circuit (see legend). Oscillations at 2.213 GHz frequency are reached at a threshold power of -4 dBm.

When the probe input power is increased to -4 dBm, the loop voltage reaches an oscillation threshold. At the highest attainable power of 9.1 dBm, oscillations are observed with a primary frequency of 2.213 GHz. That frequency matches the maximum electrical power transmission through the SAW-photonic device (Fig. 4). The full width at half maximum of the output voltage spectrum is 35 kHz. The suppression of longitudinal mode sidebands is at least 12 dB. The spectral background between the longitudinal modes peaks is 32 dB weaker than the primary peak. Harmonic distortions were at least 67 dB below the main peak (not shown).

The oscillations depend on the precise temperature tuning of the probe wavelength. They are the strongest when that wavelength is aligned with a maximum slope of the resonator

transfer function of optical power (see Fig. 3). At that alignment, the conversion of photoelastic phase modulation of the probe wave to an intensity reading is the most efficient. Figure 6 shows the radio-frequency spectrum of the loop signal for different probe wavelength. The input power of the probe wave was 9.8 dBm. With the wavelength off resonance (1544.393 nm), broadband noise background is observed, similar to traces acquired below threshold in Fig. 5. Oscillations emerge and become stronger as the probe wavelength is gradually tuned to the maximal spectral slope (1544.405 nm).

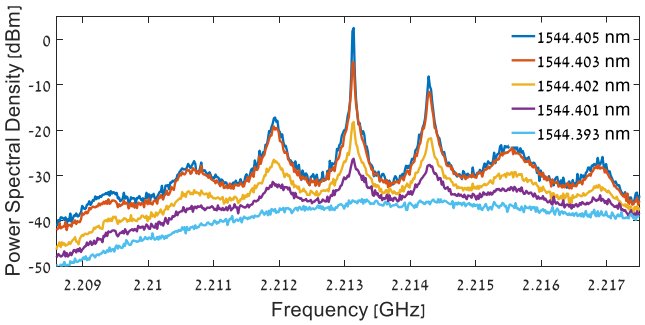

Fig. 6. Measured power spectral density of the loop output signal, for different wavelengths of the probe wave (see legend). Oscillations emerge and increase as the wavelength is scanned from outside a transmission resonance towards the maximum spectral slope of the resonator response.

IV. Summary

In this work, we have proposed and demonstrated a microwave-frequency, electro-opto-mechanical oscillator based on a standard silicon-photonic integrated device. The frequency of operation is determined by the thermoelastic actuation of SAWs on the non-piezoelectric substrate. Oscillations were obtained at a main frequency of 2.213 GHz, with 35 kHz linewidth, sidemode suppression of at least 12 dB, and harmonic distortion of -67 dB at most. The results successfully carry over previous demonstrations of an electro-opto-mechanical oscillators in optical fiber platforms [17,18] to integrated photonics. The frequency of operation is higher than those of typical quartz micro-balance devices.

The obtained linewidth, side-mode suppression, and noise levels are rather modest. Performance metrics are limited by large losses in the thermoelastic actuation of SAWs, which mandate large and noisy electrical gain. The performance can be improved through optimization of the metallic grating elements and their embedding in the substrate, and by more efficient coupling of probe light to and from the photonic circuit. To improve the performance further, laser diode sources, modulators, and detectors can be integrated on-chip, as well as part of the associated electronics.

The proposed devices can be suitable for integrated microwave-photonics signal processing applications [19,20], and for thin layers analysis on top of photonic circuits [13]. The linewidths of oscillations are 200 times narrower than those of micro-wave photonic filters based on our SAW devices [11-14]. The oscillators demonstrated herein could therefore enhance the precision of SAW-photonic thin layer analysis two hundred-fold. Compared with quartz micro-balance devices, the higher acoustic frequency can support the analysis of thin deposited layer with better precision. In conclusion, we have introduced a new microwave oscillator device to integrated silicon photonics. Future work will be dedicated to improving the oscillator performance and to analysis of thin layers.

References

[1] X. S. Yao and L. Maleki, “Optoelectronic microwave oscillator,” J. Opt. Soc. Amer. B, vol. 13, no. 8, pp. 1725–1735, Aug. 1996.

[2] X. S. Yao and L. Maleki, “Multiloop optoelectronic oscillator,” IEEE J. Quantum Electron., vol. 36, no. 1, pp. 79–84, Jan. 2000.

[3] D. Eliyahu, D. Seidel, and L. Maleki, “RF amplitude and phase-noise reduction of an optical link and an opto-electronic oscillator,” IEEE Trans. Microw. Theory Techn., vol. 56, no. 2, pp. 449–456, Feb. 2008.

[4] M. Merklein, B. Stiller, I. V. Kabakova, U. S. Mutugala, K. Vu, S. J. Madden, B. J. Eggleton, and R. Slavík, “Widely tunable, low phase noise microwave source based on a photonic chip,” Opt. Lett., vol. 41, no. 20, pp. 4633-4636, Oct. 2016.

[5] L. Maleki, “The optoelectronic oscillator,” Nature Photon., vol. 5, no. 12, pp. 728–730, Dec. 2011

[6] J. Tang, T. Hao, W. Li, D. Domenech, R. Baños, P. Muñoz, N. Zhu, J. Capmany, and M. Li, “Integrated optoelectronic oscillator,” Opt. Express, vol. 26, no. 9, pp. 12257-12265, Apr. 2018.

[7] W. Zhang, and J.Yao, “Silicon Photonic Integrated Optoelectronic Oscillator for Frequency-Tunable Microwave Generation,” J. Lightwave Technol., vol. 36, no. 19, pp. 4655-4663, Oct. 2018.

[8] P. T. Do, C. Alonso-Ramos, X. Le Roux, I. Ledoux, B. Journet, and E. Cassan, “Wideband tunable microwave signal generation in a silicon-micro-ring-based optoelectronic oscillator,” Sci. Rep., vol. 10, 6982, Apr. 2020.

[9] S. Shiokawa and J. Kondoh, “Surface acoustic wave sensors,” Jpn. J. Appl. Phys., vol. 43, no. 5B, pp. 2799–2802, May 2004.

[10] D. T. Bell and R. C. M. Li, “Surface-acoustic-wave resonators,” Proc. IEEE, vol. 64, no. 5, pp. 711–721, May 1976.

[11] D. Munk, M. Katzman, M. Hen, M. Priel, M. Feldberg, T. Sharabani, S. Levy, A. Bergman, and A. Zadok, “Surface acoustic wave photonic devices in silicon on insulator,” Nat. Commun., vol. 10, 4214, Sep. 2019.

[12] M. Katzman, D. Munk, M. Priel, E. Grunwald, M. Hen, N. Inbar, M. Feldberg, T. Sharabani, R. Zektzer, G. Bashan, M. Vofsi, U. Levy, and A. Zadok, “Surface acoustic microwave photonic filters in standard silicon-on-insulator,” Optica, vol. 8, no. 5, pp. 697–707, May 2021.

[13] M. Hen, L. Dokhanian, E. Grunwald, M. Slook, M. Katzman, M. Priel, O. Girshevitz, and A. Zadok, “Analysis of thin layers using surface acoustic wave-photonic devices in silicon-on-insulator,” Opt. Express, vol. 30, pp. 6949-6959, Feb. 2022.

[14] M. Katzman, M. Priel, I. Shafir, S. Kumar Bag, D. Munk, N. Inbar, M. Feldberg, T. Sharabani, L. Dokhanian, M. Slook, and A. Zadok, “Surface acoustic wave photonic filters with a single narrow radio-frequency passband in standard silicon on insulator,” Photon. Res., vol. 10, no. 7, pp. 1723-1730, Jul. 2022.

[15] C. Giannetti, B. Revaz, F. Banfi, M. Montagnese, G. Ferrini, F. Cilento, S. Maccalli, P. Vavassori, G. Oliviero, E. Bontempi, L. E. Depero, V. Metlushko, and F. Parmigiani, “Thermomechanical behavior of surface acoustic waves in ordered arrays of nanodisks studied by near-infrared pump-probe diffraction experiments,” Phys. Rev. B., vol. 76, no. 12, 125413, Sep. 2007.

[16] D. Nardi, M. Travagliati, M. E. Siemens, Q. Li, M. M. Murnane, H. C. Kapteyn, G. Ferrini, F. Parimgiani, and F. Banfi, “Probing thermomechanics at the nanoscale: impulsively excited pseudosurface acoustic waves in hypersonic phononic crystals,” Nano Lett., vol. 11, no. 10, pp. 4126–4133, Sep. 2011.

[17] Y. London, H. H. Diamandi, and A. Zadok, “Electro-opto-mechanical radio-frequency oscillator driven by guided acoustic waves in standard single-mode fiber,” Appl. Phys. Lett. – Photon., vol. 2, 041303, Mar. 2017.

[18] H. H. Diamandi, Y. London, G. Bashan, A. Bergman, and A. Zadok, "Highly-coherent stimulated phonon oscillations in a multi-core optical fibers," Sci. Rep., vol. 8, 9514, Jun. 2018.

[19] D. Marpaung, C. Roeloffzen, R. Heideman, A. Leinse, S. Sales, and J. Capmany, “Integrated microwave photonics,” Laser Photon. Rev., vol. 7, no. 4, pp. 506–538, Jan. 2013.

[20] D. Marpaung, J. Yao, and J. Capmany, “Integrated microwave photonics,” Nat. Photon., vol. 13, no. 2, pp. 80–90, Feb. 2019.